Inorg. Chem. **2009**, *48*, 204−208

New $A_{2/3-x}Rh_2O_4$ Compounds with the $CaFe_2O_4$ Structure Where A Is a Rare Earth or Bi

Hiroshi Mizoguchi,[†] L. N. Zakharov,[†] A. P. Ramirez,[‡] W. J. Marshall,[§] A. W. Sleight,[†] and M. A. Subramanian*,[†]

Department of Chemistry and Oregon University Materials Institute, Oregon State University, Corvallis, Oregon 97331-4003, Bell Laboratories, Alcatel−Lucent, 600 Mountain Avenue, Murray Hill, New Jersey 07974, and Central Research and Development, Dupont Company, Experimental Station, Wilmington, Delaware 19880-0228

Received August 25, 2008

New compounds of the type $R_{2/3-x}Rh_2O_4$ with the $CaFe_2O_4$ structure have been prepared, where R is a rare earth. For crystals grown in a Bi/V/O flux, the rare earth was partially replaced by Bi. No evidence of ordering of the A cation vacancies is found, but the A cations are displaced from the ideal A cation site by about 0.24 Å. Electrical conductivity measurements on crystals suggest that the materials are degenerate semiconductors with Seebeck measurements showing p-type behavior. This is consistent with our observation that *x* in $R_{2/3-x}Rh_2O_4$ ranges up to about 0.09. The compounds were also characterized by magnetic susceptibility and diffuse reflectance measurements.

1. Introduction

The $CaFe_2O_4$ structure is well-known among AM_2O_4 oxides.[1] This structure may be regarded as being based on MO_6 octahedra, which share edges and corners to form a network where the A cations residing in the channels are in 8-fold coordination. It has been known since 1970 that $CaRh_2O_4$ forms in this structure.[2] Recently, other Rh oxides reported with the $CaFe_2O_4$ structure are $Cu_{0.96}Bi_{0.04}Rh_2O_4$, $(Ca,Na)Rh_2O_4$, and $CuRh_2O_4$, the latter two compounds being prepared at high pressure.[3−5] The A site in the $CaFe_2O_4$ structure is normally fully occupied, but partial occupancy is reported for $Na_{0.56}Ti_{0.28}Fe_{1.72}O_4$, $Li_{0.8}Mn_2O_4$, and $Ca_{2/3}Mn_2O_4$.[6−8] In this paper, we report some new nominally $A_{2/3}Rh_2O_4$ compounds with the $CaFe_2O_4$ structure where A may be a rare earth or a mixture of a rare earth and Bi.

2. Experimental Section

The reactants were Bi_2O_3 (99.9%, Baker), V_2O_5 (99.9%, Johnson Matthey), Y_2O_3 (99.99%, Research Chemicals), La_2O_3 (99.999%, AlfaAesar), Pr_6O_{11} (Research Chemicals), Nd_2O_3 (99.9%, Research Chemicals), Sm_2O_3 (99.99%, REacton), Eu_2O_3 (99.9%, Johnson Matthey), Gd_2O_3 (99.99%, Research Chemicals), Tb_4O_7 (99.99%, Research Chemicals), Dy_2O_3 (99.99%, Research Chemicals), Ho_2O_3 (99.9%, Aldrich), Er_2O_3 (99.99%, Aldrich), Tm_2O_3 (99.9%, Aldrich), Yb_2O_3 (99.9%, Aldrich), Lu_2O_3 (99.99%, Research Chemicals), $CaCO_3$ (99.0%, Spectrum Chemical MFG Corp.), and Rh_2O_3 prepared from $RhCl_3 \cdot xH_2O$ (99.9%, Alfa Aesar) by heating in moist air at 1073 K for 10 h. R oxides were also heated at 1273 K for 5 h, before weighing. Approximate amounts of R oxides and Rh_2O_3 were mixed by grinding them together under ethanol in an agate mortar. This pressed mixture was placed in an alumina boat and heated under O_2 at 1173 K and then at1273 K each for 20 h with intermediate grinding.

Single crystals of $(R_{1-y}Bi_y)_{2/3-x}Rh_2O_4$ compounds were grown in a flux of 75% Bi_2O_3−25% V_2O_5. An intimate mixture of the R oxide (about 0.04 g), Rh_2O_3 (0.030 g), Bi_2O_3 (0.400 g), and V_2O_5 (0.044 g) was heated to 1373 K under air in a covered alumina

* Author to whom correspondence should be addressed. Fax: 541-737-8235. E-mail: mas.subramanian@oregonstate.edu.
[†] Oregon State University.
[‡] Alcatel−Lucent.
[§] Dupont Company.

(1) Muller-Buschbaum, H. *J. Alloys. Compd.* **2003**, *349*, 49.
(2) Preudhomme, J.; Chaudron, M. G. *C. R. Acad. Sci. Paris, Sec. C* **1970**, *271*, 1073.
(3) Renkenberger, C. Ph. D thesis, University of Heidelberg, Germany, 2004.
(4) Yamaura, K.; Huang, Q.; Moldovan, M.; Young, D. P.; Sato, A.; Baba, Y.; Nagai, T.; Matsui, Y.; Takayama-Muromachi, E. *Chem. Mater.* **2005**, *17*, 359.
(5) Ohgushi, K.; Gotou, H.; Yagi, T.; Ueda, Y. *J. Phys. Soc. Jpn.* **2006**, *75*, 023707.
(6) Ishiguro, T.; Tanaka, K.; Marumo, F.; Ismail, M. G. M. U.; Hirano, S.; Somiya, S. *Acta Crystallogr.* **1978**, *34B*, 3346.
(7) Yamaura, K.; Huang, Q.; Zhang, L.; Takada, K.; Baba, Y.; Nagai, T.; Matsui, Y.; Kosuda, K.; Takayama-Muromachi, E. *J. Am. Chem. Soc.* **2006**, *128*, 9448.
(8) Hadermann, J.; Abakumov, A. M.; Gillie, L. J.; Martin, C.; Hervieu, M. *Chem. Mater.* **2006**, *18*, 5530.

10.1021/ic801603t CCC: $40.75
Published on Web 12/02/2008

Table 1. Orthorhombic Unit Cell Parameters for $(R_{1-y}Bi_y)_{2/3-x}Rh_2O_4$ Compounds

formula	*a*, Å	*b*, Å	*c*, Å	*V*, Å^3
$(Y_{1-y}Bi_y)_{2/3-x}Rh_2O_4$	9.103(6)	3.032(2)	10.786(6)	297.7(4)
$Pr_{2/3-x}Rh_2O_4$	9.156(2)	3.046(1)	10.900(1)	304.0(1)
$(Sm_{1-y}Bi_y)_{2/3-x}Rh_2O_4$	9.139(4)	3.048(2)	10.869(3)	302.5(2)
$Eu_{0.58}Rh_2O_4$	9.095(2)	3.036(1)	10.838(2)	299.3(1)
$Gd_{2/3-x}Rh_2O_4$	9.073(2)	3.028(1)	10.824(3)	297.4(1)
$Ho_{2/3-x}Rh_2O_4$	9.008(1)	3.038(1)	10.770(1)	294.7(1)
$(Er_{0.52}Bi_{0.48})_{0.67}Rh_2O_4$	9.0556(13)	3.0181(4)	10.7809(15)	294.65(7)
$(Tm_{1-y}Bi_y)_{2/3-x}Rh_2O_4$	9.043(4)	3.020(2)	10.767(4)	294.0(2)
$(Lu_{1-y}Bi_y)_{2/3-x}Rh_2O_4$	9.025(3)	3.012(2)	10.770(4)	293.3(2)

Table 2. Crystallographic Data for $(R_{1-y}Bi_y)_{2/3-x}Rh_2O_4$ Crystals

A	$(Nd_{0.58}Bi_{0.42})_{0.63}$	$(Eu_{0.59}Bi_{0.41})_{0.64}$	$(Yb_{0.72}Bi_{0.28})_{0.67}$
fw	374.85	382.37	392.90
Space group	*Pnma*	*Pnma*	*Pnma*
a/Å	9.1521(7)	9.1109(8)	9.0337(10)
b/Å	3.0483(2)	3.0402(3)	3.0164 (4)
c/Å	10.8929(8)	10.8497(9)	10.7557(12)
V/Å^3	303.89(4)	300.53(5)	293.08(6)
ρ_{calcd}/g cm^{-3}	8.196	8.444	8.895
μ/mm^{-1}	26.72	33.84	37.49
R(*F*)	0.0173	0.0229	0.0206
$R_w(F_0^2)$	0.0413	0.0454	0.0476

Table 3. Selected Bond Distances (Å) for $(R_{1-y}Bi_y)_{2/3-x}Rh_2O_4$

	Nd	Eu	Yb
Rh(1)−O(3)*2	2.023(3)	2.019(5)	1.999(3)
Rh(1)−O(4)	2.032(4)	2.041(8)	2.023(5)
Rh(1)−O(4)*2	2.044(3)	2.047(5)	2.049(3)
Rh(1)−O(1)	2.081(4)	2.073(7)	2.061(5)
Rh(2)−O(3)	2.047(4)	2.031(7)	2.011(5)
Rh(2)−O(2)*2	2.039(3)	2.040(5)	2.043(4)
Rh(2)−O(2)	2.041(4)	2.051(7)	2.050(5)
Rh(2)−O(1)*2	2.068(3)	2.067(5)	2.061(3)
R/Bi−O(4)	2.268(3)	2.242(6)	2.198(4)
R/Bi−O(2)	2.308(3)	2.287(6)	2.248(4)
R/Bi−O(1)	2.346(3)	2.324(6)	2.283(4)
R/Bi−O(3)	2.512(4)	2.504(8)	2.482(6)
R/Bi−O(3)	2.552(4)	2.540(8)	2.529(6)
R/Bi−O(4)	2.573(3)	2.541(6)	2.488(4)
R/Bi−O(2)	2.609(3)	2.581(6)	2.532(4)
R/Bi−O(2)	2.642(3)	2.614(5)	2.564(4)

crucible. After holding for 10 h, the crucible was cooled to 973 K at a rate of 5 K/h. After reaching 973 K, it was cooled to room temperature at a rate of 200 K/h. The flux was dissolved in HNO_3 (aq) at 360 K. The photo for $(Eu_{0.59}Bi_{0.41})_{0.64}Rh_2O_4$ crystals is shown in Figure S1 (Supporting Information). The products are consisted of black shiny needle crystals 0.5−3 mm in length.

The cationic composition for single crystals was determined using a CAMECA SX100 electron microprobe analyzer. No vanadium could be detected in the crystals. Single-crystal X-ray diffraction data were collected on a Bruker SMART APEX CCD system at 173 K using Mo Kα radiation ($\lambda = 0.71073$ Å). The Bruker Saint program[9] was used for integration. Absorption corrections were applied by SADABS.[9] The crystal structure was solved by direct methods and refined with the full-matrix least-squares method on F^2. The final refinements for the Nd, Eu, and Yb complexes were done on the basis of the microprobe analysis data for these compounds. All calculations were performed using the Bruker SHELXTL package.[9] Further details for data collections and the crystal data are given in Tables 1−3, and in available CIF files. X-ray powder diffraction patterns were obtained with a RIGAKU MINIFLEX II apparatus with Cu Kα radiation and a NiK_β filter. Si (5N) was used as the internal standard to determine the lattice constants.

DC electrical conductivity measurements were conducted using a conventional four-probe method over the temperature region 80−300 K. Seebeck coefficient measurements were obtained over the temperature region 120−300 K. Magnetic measurements were made using a Quantum Design Magnetic Properties Measurement System. Diffuse reflectance spectra of powdered samples were obtained in the region 400−1100 nm using a W halogen lamp and a grating double monochromator as the source. The diffuse light reflected by the powders was collected with an integration sphere and detected with a Si diode detector. MgO was used as a reference. The data were transformed into absorbance using the Kubelka−Munk function.

3. Results

Strong XRD patterns of a $CaFe_2O_4$-type phase were obtained upon attempts to prepare compounds of the $R_{2/3}Rh_2O_4$ composition where R = Pr, Sm, Eu, Gd, Ho, Tm, or Y. However, a small amount of perovskite-type $RRhO_3$ was invariably present. This indicated that the real composition of the $CaFe_2O_4$-type phases is $R_{2/3-x}Rh_2O_4$. This was confirmed by analytical data and the observed electrical properties. Thus, pure $CaFe_2O_4$-type phases could be obtained by decreasing the R/Rh reactant ratio. For example, in the case of R = Eu, a pure phase with a bluish black color was obtained for the composition with Eu/Rh = 0.58:2. This color suggests metallic properties with an average oxidation state of Rh higher than 3. As the size of R decreased, the amount of perovskite phase impurity decreased, indicating that *x* in $R_{2/3-x}Rh_2O_4$ was decreasing. In the case of R = Y, a dark brown pellet was obtained, indicating that *x* is small. Attempts to prepare a $CaFe_2O_4$-type phase with R = La were unsuccessful. The $R_{2/3-x}Rh_2O_4$ phases decomposed into $RRhO_3$ and Rh metal upon heating to 1100 C in the air. Single crystals with the $CaFe_2O_4$-type structure were readily obtained in the Bi/V/O flux, but microprobe analysis on these crystals always indicated the incorporation of Bi.

The structure for the $A_{2/3-x}$ Rh_2O_4 phases is shown in Figure 1a, and values of the unit cell edges and volumes are given in Tables 1 and 2. The structure consists of edge-shared RhO_6 octahedra running along *b* axis. Two chains share edges of octahedra with each other, forming double chains that are linked by octahedra sharing corners. In the refinement, the ratio of Bi/R in the A site was fixed on the basis of the microprobe analysis data for these crystals. Total occupancy of the A ion (*x* value) was refined along with other parameters. Results for three crystals are given in Tables 2 and 3. Details are given in available CIF files. Neither X-ray powder patterns of $R_{2/3-x}Rh_2O_4$ phases nor X-ray single-crystal diffraction of $(R_{1-y}Bi_y)_{2/3-x}Rh_2O_4$ phases showed any evidence of a superstructure. Thus, there is no evidence for three-dimensional ordering of the A cation vacancies. Figure 2 shows the temperature dependence of electrical conductivity along the *b* axis for two crystals. Also given are the Seebeck coefficients for two sintered bars. Magnetic susceptibility data are presented is Figure 3. Diffuse reflectance spectra for three phases are compared to that of $LuRhO_3$ in Figure 4. A bandgap is observed for $LuRhO_3$, which has a

(9) *SMART*, version 5.054; Bruker Analytical X-ray Instruments, Inc.: Madison, WI, 2003.

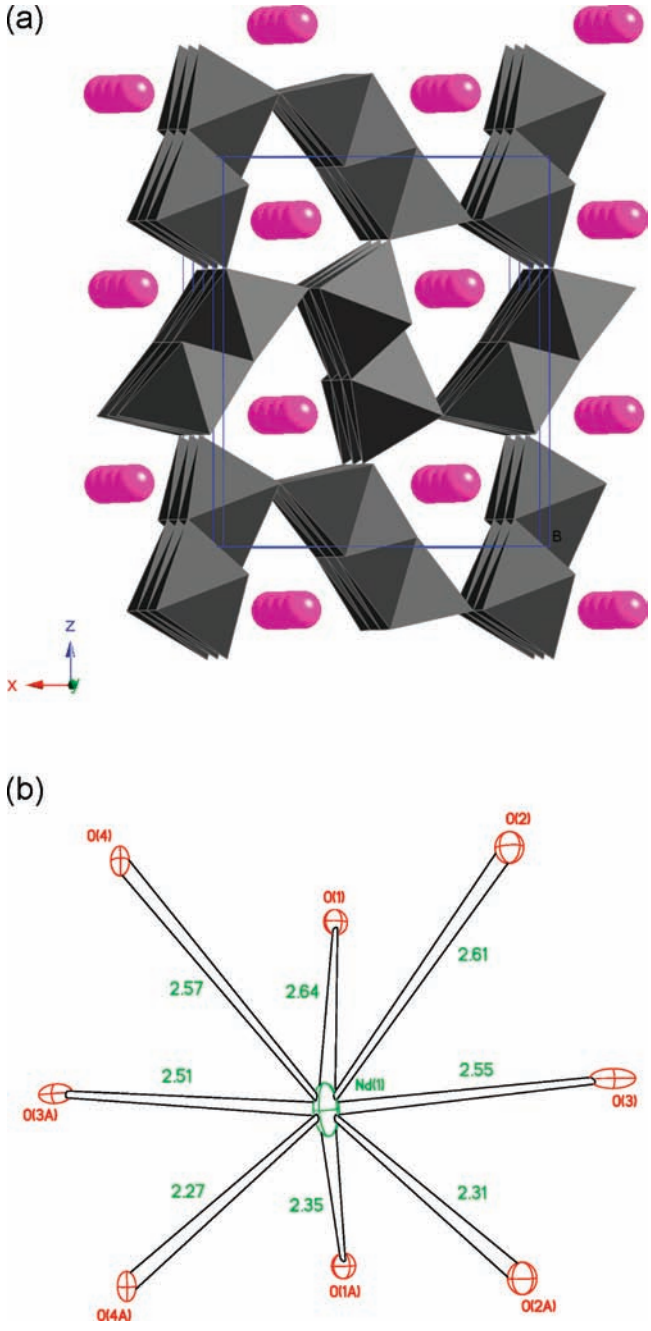

Figure 1. (a) The structure for the $A_{2/3-x}Rh_2O_4$ phases. (b) Coordination of the A cation in $(Nd_{0.58}Bi_{0.42})_{0.63}Rh_2O_4$ with bond distances (Å; a view along the *y* axis).

low-spin $4d^6$ closed shell, as reported by Jarrett et al.[10] No clear absorption edge is observed for the $R_{2/3-x}Rh_2O_4$ oxides, which is consistent with their apparent high carrier concentration.

4. Discussion

In the ideal $CaFe_2O_4$ structure, all atoms lie on the mirror plane in position 4c of space group *Pnma*. For the $(R_{1-y}Bi_y)_{2/3-x}Rh_2O_4$ phases, all atoms are on the mirror plane in space group *Pnma* except for the A cation. The displacement of the A cation off the mirror plane is about 0.24 Å for the three structures refined. The A cation occupancy of this 8d site is about 33%. The two sites immediately adjacent to the mirror plane are too close (~0.5 Å) to be simultaneously occupied. We may thus consider the occupancy of the plausible A sites in this chain to be about 67%. The shortest A−A distance between chains is nearly 5 Å, whereas the A−A distances in the chains between 4c positions are about 3 Å. Electrostatics thus dictates that every third A cation position along the *b* axis will be vacant. Electrostatic considerations would also cause the A cations to be displaced toward the vacant site, as shown in Figure S2 (Supporting Information). With no A cation displacement off the mirror plane, the A−A distances along the *b* axis would all be 3.05 Å. With the vacancies and the ordered displacements shown in Figure S2, the A−A distances along this chain become 3.53 and 5.61 Å. The one-dimensional order shown in Figure S2 may well be very high, but the absence of a superstructure along the *b* axis indicates that any vacancy ordering is not three-dimensional in nature. In $Ca_{2/3}Mn_2O_4$, there is complete three-dimensional ordering of the A cation vacancies with a situation very similar to what we find in the $(R_{1-y}Bi_y)_{2/3-x}Rh_2O_4$ phases.[8] The Ca atoms are displaced 0.235 Å from the positions they would have in the ideal $CaFe_2O_4$ structure. Thus, the Ca−Ca distances become 3.30 and 5.19 Å instead of the 2.83 Å value they would have in the ideal $CaFe_2O_4$ structure. In the case of $Ca_{2/3}Mn_2O_4$, there is also charge ordering of Mn^{3+} and Mn^{4+}. The lack of three-dimensional order of the A cation vacancies in our $R_{2/3-x}Rh_2O_4$ and $(R_{1-y}Bi_y)_{2/3-x}Rh_2O_4$ phases may be caused by the deviation from the ideal $A_{2/3}M_2O_4$ stoichiometry. The charge-ordered structure of $Ca_{2/3}Mn_2O_4$ provides distorted octahedral sites for Mn^{3+}. There is, however, no driving force to provide any distorted octahdral sites in $R_{2/3-x}Rh_2O_4$ and $(R_{1-y}Bi_y)_{2/3-x}Rh_2O_4$ phases. This can be another reason for the lack of complete charge ordering in the $R_{2/3-x}Rh_2O_4$ and $(R_{1-y}Bi_y)_{2/3-x}Rh_2O_4$ phases.

The A cation coordination for $(Nd_{0.58}Bi_{0.42})_{0.63}Rh_2O_4$ is shown in Figure 1b. Without the A cation displacement off the mirror plane, the two A−O1 distances would be equal, the two A−O2 distances would be equal, and the two A−O4 distances would be equal. The thermal ellipsoid elongation of the A cation along the *b* axis observed for all of our $(R_{1-y}Bi_y)_{2/3-x}Rh_2O_4$ phases is likely caused primarily by slightly different *y* values for the A cation, depending on whether A is Bi or the rare earth cation.

The conductivity values of the $(R_{1-y}Bi_y)_{2/3-x}Rh_2O_4$ phases (Figure 2) coupled with the weak temperature dependence of the conductivity suggest that these materials could be regarded as degenerate semiconductors. This description is consistent with the relatively high Seebeck coefficients (Figure 2). The valence and conduction bands in Rh^{3+} oxides are the filled 4d t_{2g} and empty 4d e_g bands, respectively. It is well-known that such oxides can normally be doped p- or n-type.[10] The positive values of the Seebeck coefficients for the $R_{2/3-x}Rh_2O_4$ phases indicate that they are all p-type. The trend of the unit cell volumes (Tables 1 and 2) is consistent with the usual lanthanide contraction, indicating that all R cations are in the trivalent state. Thus, the sign of Seebeck

(10) Jarrett, H. S.; Sleight, A. W.; Kung, H. H.; Gilson, J. L. *J. Appl. Phys.* **1980**, *51*, 3916.

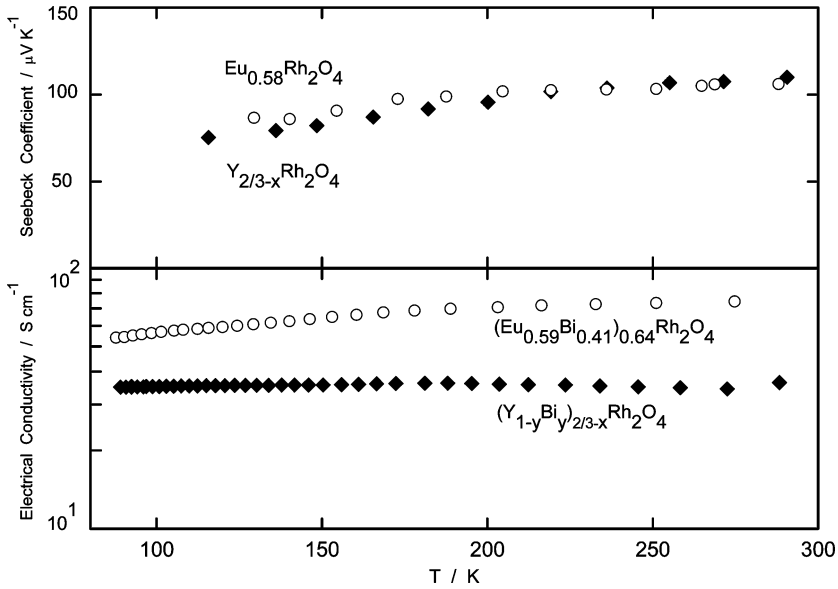

Figure 2. Temperature dependence of electrical conductivity along the *b* axis for two crystals. Also given are the Seebeck coefficients for two sintered bars.

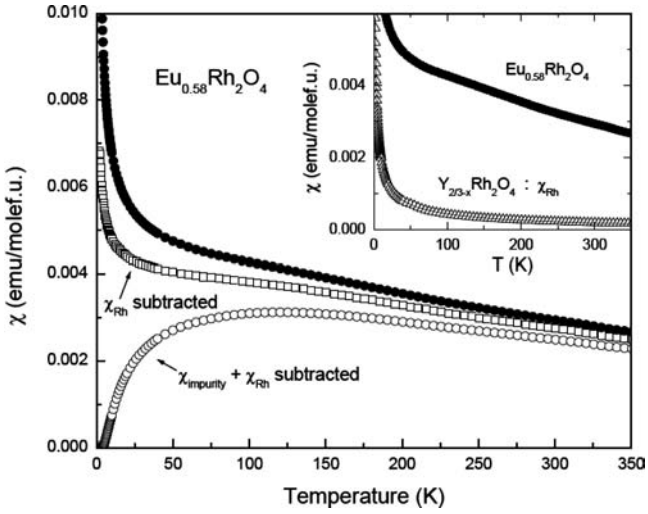

Figure 3. Magnetic susceptibility data for $Eu_{0.58}Rh_2O_4$. The filled circles are raw data. The open squares have the fit to the $Y_{2/3-x}Rh_2O_4$ data, χ_{Rh}, subtracted. The open circles also have a Curie−Weiss term approximating impurity spins subtracted. Inset: Magnetic susceptibility data for $Eu_{0.58}Rh_2O_4$ and $Y_{2/3-x}Rh_2O_4$. For the molar calculation, the x value for $Y_{2/3-x}Rh_2O_4$ was set to zero. The $Y_{2/3-x}Rh_2O_4$ data have been fit to a two-spin population model described in the text.

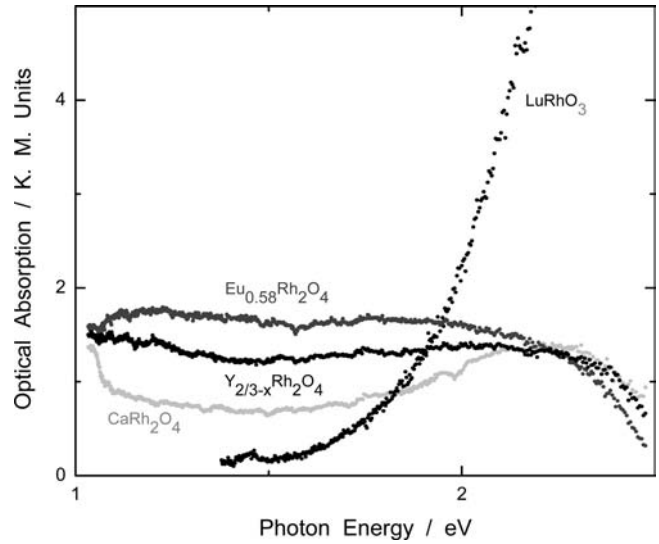

Figure 4. Diffuse reflectance spectra for two $R_{2/3-x}Rh_2O_4$ phases compared to that of $CaRh_2O_4$ and $LuRhO_3$.

Table 4. Fitting Parameters to the Two-Spin Curie−Weiss Formula for $Y_{2/3-x}Rh_2O_4$

θ/K	−1.18	−108.84
C/emu K/mol f. u.	0.00855	0.0295
μ_{eff}	0.26 μ_B	0.49 μ_B

coefficients is consistent with our $R_{2/3-x}Rh_2O_4$ formulation for these phases. The high optical absorption throughout the visible region indicates a high doping level. These phases can also be considered as mixed valent oxides containing both Rh^{3+} and Rh^{4+}. The magnetic susceptibility, $\chi(T)$, for both compounds is shown in the inset to Figure 3. The larger magnitude of $\chi(T)$ for $Eu_{0.58}Rh_2O_4$ is most likely due to the magnetism of Eu, as discussed below. In order to separate the contributions to $\chi(T)$ from the Rh and Eu ions, we first fit the data for $Y_{2/3-x}Rh_2O_4$. Here, Y is expected to be nonmagnetic, and thus, $\chi(T)$ is determined by Rh only. As can be seen in the inset to Figure 3, $\chi(T)$ for $Y_{2/3-x}Rh_2O_4$ is dominated by a low-temperature contribution. Above 100 K, however, the temperature dependence is still significant; thus, a single Curie−Weiss (C−W) term could not accurately fit the data. We found that two distinct C−W terms provide an excellent fit, χ_{Rh}, over the entire temperature range, 2−350 K, and the fit parameters are shown in Table 4. We then subtracted these data on a mole-formula-unit basis from the $\chi(T)$ of $Eu_{0.58}Rh_2O_4$, with the result shown in Figure 3 as the open squares. This $\chi(T)$, ostensibly due only to Eu magnetism, is clearly not described by a single C−W term. Subtracting a C−W fit ($C = 0.1376$ emu K/mol, $\theta = -9.70$ K in the temperature region 2−5 K) to the lowest temperature data from the full data set yields the open circle symbols in Figure 3. Since the $4f^6$ configuration of Eu^{3+} is non-Kramers, there will be no low-temperature magnetism, and thus the resulting broad peak in $\chi(T)$ is most likely due to the $J = 1$

excited state. Of most interest, however, are the results of the C−W fits. The fit, χ_{Rh}, for $Y_{2/3-x}Rh_2O_4$ produces two sets of spins, with effective moments of 0.26 and 0.49 μ_B, implying densities of spin 1/2 moments of 2.2% and 7.9% on a molar basis. Thus, the magnetism of Rh in this compound is equivalent to that of ~10% spin 1/2's, which, if due to Rh^{4+}, means the compound should be expressed as $Y_{0.60}Rh^{3+}_{1.8}Rh^{4+}_{0.2}O_4$.

No free-spin paramagnetism is expected for Eu^{3+}, as mentioned above. A somewhat higher Rh-derived moment can be expected however for $Eu_{0.58}Rh_2O_4$ relative to $Y_{0.60}Rh_2O_4$ due to a higher Rh^{4+} concentration caused by an small increase in the A cation vacancy concentration. However, there cannot be enough Rh^{4+} to account for the observed moment in $Eu_{0.58}Rh_2O_4$, assuming that the moment on Rh^{4+} does not have a significant orbital contribution. The possibility of a significant orbital contribution from Rh^{4+} is based on previous results we obtained for $(Bi_6O_5)Rh_{12}O_{24}$.[11] Another possibility for the high moment for $Eu_{0.58}Rh_2O_4$ is that some Eu is present as Eu^{2+}. In the case of $EuRhO_3$, paramagnetism that was not expected for a Eu^{3+}/Rh^{3+} combination was found.[12] The authors suggest admixing of Eu^{2+}/Rh^{4+} with Eu^{3+}/Rh^{3+} complexes, which is unexpected since one normally expects Eu^{2+} to reduce Rh^{4+} to Rh^{3+}. In the case of $Eu_{0.58}Rh_2O_4$, however, it is easier to rationalize the existence of some Eu^{2+} in the presence of Rh^{4+}. Although we have proposed a high degree of order in the A cation chains (Figure S2), the lack of three-dimensional order indicates that significant one-dimensional disorder exists. If one of the normally vacant A cation sites is occupied by Eu, there would be an electrostatic push for this Eu to be Eu^{2+} rather than Eu^{3+}. We have analyzed our data on the basis that the increased moment in $Eu_{0.58}Rh_2O_4$ relative to $Y_{0.60}Rh_2O_4$ is due to the presence of Eu^{2+}. The low-temperature C−W fit to $\chi(T)$ of $Eu_{0.58}Rh_2O_4$ with χ_{Rh} subtracted is possibly due to low levels of Eu^{2+} impurities. Since Eu^{2+} is $4f^7$ with $S = 7/2$, the fit yields a density of such spins of 1.75%, which is a reasonably small density of impurity spins.

Acknowledgment. The research was supported by a grant from National Science Foundation (DMR-0804167). We are grateful to Dr. J. Tate for assistance with the optical measurements.

Supporting Information Available: Additional figures (PDF) and crystallographic information (CIF). This material is available free of charge via the Internet at http://pubs.acs.org.

IC801603T

(11) Mizoguchi, H.; Marshall, W. J.; Ramirez, A. P.; Sleight, A. W.; Subramanian, M. A. *J. Solid State Chem.* **2007**, *180*, 3463.
(12) Taniguchi, T.; Iizuka, W.; Nagata, Y.; Uchida, T.; Samata, H. *J. Alloys Comp.* **2003**, *350*, 24.